

CrossDehaze: Scaling Up Image Dehazing with Cross-Data Vision Alignment and Augmentation

Yukai Shi[†], Zhipeng Weng[†], Yupei Lin, Cidan Shi, Xiaojun Yang, and Liang Lin, *Fellow, IEEE*

Abstract—In recent years, as computer vision tasks have increasingly relied on high-quality image inputs, the task of image dehazing has received significant attention. Previously, many methods based on priors and deep learning have been proposed to address the task of image dehazing. Ignoring the domain gap between different data, former de-hazing methods usually adopt multiple datasets for explicit training, which often makes the methods themselves be violated. To address this problem, we propose a novel method of internal and external data augmentation to improve the existing dehazing methodology. By using cross-data external augmentor. The dataset inherits samples from different domains that are firmly aligned, making the model learn more robust and generalizable features. By using the internal data augmentation method, the model can fully exploit local information within the images, thereby obtaining more image details. To demonstrate the effectiveness of our proposed method, we conduct training on both the Natural Image Dataset (NID) and the Remote Sensing Image Dataset (RSID). Experimental results show that our method clearly resolves the domain gap in different dehazing datasets and presents a new pipeline for joint training in the dehazing task. Our approach significantly outperforms other advanced methods in dehazing and produces dehazed images that are closest to real haze-free images. The code will be available at: <https://github.com/wengzp1/ScaleUpDehazing>

Index Terms—Image Dehazing, Vision Alignment, Vision Augmentation, Remote Sensing, Self-Supervised Learning.

I. INTRODUCTION

IN the field of remote sensing images and natural images, haze usually leads to a decrease in image contrast and clarity. It makes the originally distinct boundaries of objects blurry, greatly affecting the visual effect of the image. Therefore, developing effective dehazing methods is of great significance for enhancing the application value of remote-sensing images. Previous dehazing methods mainly address hazy images by using atmospheric scattering models [3], [4], [5]. The model explains how light interacts with particulate matter in the atmosphere under hazy conditions, thereby affecting the imaging process of the images. The specific representation is as follows:

$$I(x) = J(x)t(x) \oplus A(1 - t(x)), \quad (1)$$

where x is a pixel position in the image, $J(x)$ represents the true haze-free image, and A is the global atmospheric light. $t(x)$ represents the medium transmission rate, which ranges from 0 to 1. Here, 0 indicates no transmission, meaning complete opacity, while 1 indicates complete transparency. $I(x)$ represents the hazy image obtained after the haze-free image undergoes atmospheric scattering.

Early dehazing methods utilize prior knowledge of the image to separately estimate the haze parameter $t(x)$ and A , and then further use the atmospheric scattering model to obtain the haze-free image $J(x)$. GDGP [6] improves the steps of estimating atmospheric light and transmission rate in the original DCP [7] by introducing new assumptions and constraints, thereby effectively estimating these parameters from hazy images. ALC [8] proposes an image dehazing method that combines atmospheric light white balance correction, local light filtering, and high-altitude perspective priors to restore clarity to hazy images. While these methods are simple and intuitive, they struggle to effectively remove haze in non-uniformly hazy images.

Recently, many methods have emerged for use in the field of image dehazing. ROP [9] introduces a rank-one matrix to represent complex scenes as linear combinations of a series of simple basic elements and then uses these basic elements for image dehazing. Cycle-SNSPGAN [10] improves the quality of dehazed images by combining spectral normalization and patch discriminator techniques. DEFADE [11] achieves perceptual prediction of haze density by analyzing the statistical features of natural scenes and haze-sensitive features in the image. In addition, some deep learning methods train on a large number of hazy and haze-free image pairs, and use models such as CNNs or Transformers to learn the mapping from hazy images to clear ones. UHD [12] proposes a multi-guided bilateral learning method, which combines features from multiple scales and levels of images as well as bilateral filtering techniques to obtain dehazed images. Dehamer [1] introduces a transmission-aware 3D positional embedding module into the Transformer, providing relative positional information while incorporating priors related to haze density. Trinity-Net [2] consists of three parameter estimation networks: the haze thickness estimator network(S-Net), the ambient light estimator network(A-Net), and the medium transmission estimator network(T-Net). Obtaining these parameters further generates dehazed images.

However, the aforementioned methods mostly consider the model perspective and rarely take the data aspect into account. The dehazing results obtained by the aforementioned methods still have limitations due to the narrow training data. Specifically, the training dataset lacks diversity in terms of scenes and types of haze, resulting in the model’s inability to achieve good robustness. Moreover, there is a domain gap between existing datasets, and directly using multiple datasets for training often results in limited performance improvement.

To address the issue of data scarcity and uniqueness, we propose a novel method of external data augmentor and

[†] The first two authors share equal contribution.

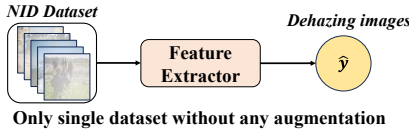

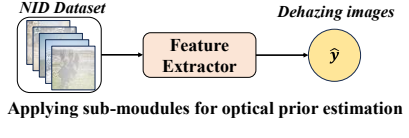
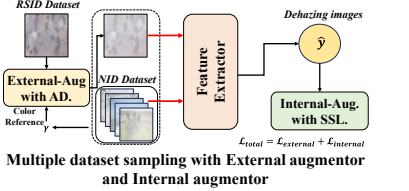

Method		Framework	Description		Comparison
Previous dehazing methods	Dehazer	 <p>Only single dataset without any augmentation</p>	<i>Dehazer is trained using only a single dataset.</i>	<i>Whether using only a single dataset or directly using multiple datasets for training, the dehazed results still have limitations.</i>	 <p>PSNR:23.15 SSIM:0.9779</p>
	Trinity-Net	 <p>Applying sub-modules for optical prior estimation</p>			<i>Trinity-Net directly uses multiple datasets for training.</i>
Ours		 <p>Multiple dataset sampling with External augmentor and Internal augmentor</p>	<i>Our method focuses on both external data augmentation and internal data augmentation. It not only reduces the domain gap between different datasets but also enables the model to learn more robust and generalizable features.</i>		 <p>PSNR:33.75 SSIM:0.9964</p>

Fig. 1: Our method compared to other dehazing methods in terms of flowchart and characteristics. From the perspective of performance and methodology, we apply Dehazer [1] and Trinity-Net [2] for comparison. Ignoring the domain gap between different data, former de-hazing methods usually adopt multiple datasets for explicit training, which often make the methods itself be violated. To address this issue, we call for the internal- and external knowledge can be further augmented with a self-supervised learning to fill up the domain gap.

internal data augmentor to improve the dehazing model. Specifically, we first expand the dataset externally using a channel alignment method. Next, we apply strong-weak augmentation methods internally and perform self-supervised learning on the resulting images within the dataset. Finally, we compare our approach with the advanced dehazing works, and the performance metrics demonstrate the superiority of our method. As shown in Fig. 1, it can be observed that our method outperforms Dehazer and Trinity-Net in terms of quantitative metrics such as PSNR and SSIM from the obtained dehazed results. Additionally, the dehazing results produced by our method visually appear closer to real haze-free images. In summary, the contributions of this paper can be summarized as follows:

- We proposed a cross-data external augmentor. The dataset inherits samples from different domains that are aligned by the external data augmentor, making the model learn more robust and generalizable features.
- We proposed an internal data augmentor in a strong-weak fashion. The model can effectively explore local information within images. While the model focuses on the overall image externally, the local details of the image also be fully explored.
- Experiments have shown that our method achieves state-of-the-art results. Our method outperforms other advanced methods in terms of PSNR and SSIM metrics.

II. RELATED WORK

A. Remote-sensing Image Dehazing

In the fields of geography and remote sensing, image dehazing techniques play an important role in image preprocessing. Due to the poor visibility of remote sensing images or natural images acquired in hazy environments, it is visually easy to cause the loss of details [7], [13]–[16]. Hazy images are not conducive to the related tasks of computer vision, thus causing a lot of challenges to a certain extent. For example, hazy images make it difficult for object detection models to accurately identify and localize objects in the images [17], [18]. In semantic segmentation tasks [19], the presence of haze makes scene boundaries that should be clear become blurred, leading to segmentation models struggling to differentiate between different objects or scene elements. In image recognition tasks [20], the presence of haze interferes with the model’s overall understanding of the image content.

The methods for dehazing remote sensing images can be mainly classified into two categories: those based on priors and those based on learning. Early, He et al. proposed the Dark Channel Prior (DCP) [7] method. They observed that in at least one color channel, there are always some pixels in local regions of the image with very low intensity. This prior is used to estimate the distribution of haze in the image. Color Attenuation Prior (CAP) [21] is a method based on physical models. It assumes that in a hazy environment, the color of a scene gradually attenuates as the depth increases. This prior can be used to estimate the depth map of the scene, thereby restoring the clear image. Color-lines [22] analyze the color information in the image to estimate the distribution of haze

and depth information of objects in the scene. Haze-lines [23] involves a deep understanding and analysis of image features under hazy conditions. By identifying hazy regions in the image and decomposing and processing them, haze-lines aim to remove the effects of haze.

Recently, with the development of deep learning techniques, deep learning-based dehazing methods have gradually become a research hotspot. DehazeNet [24] utilizes the deep architecture of CNN to output the medium transmission map. Then, it uses the atmospheric scattering model to recover the haze-free image. MSCNN [25] combines a multi-scale information extraction subnetwork and a multi-scale residual dilated convolution module. It integrates features from different receptive fields to estimate the transmission map of hazy images. DCPDN [26] employs two generators, one for generating the transmission map and the other for estimating the atmospheric light. GFN [27] processes images through operations such as white balancing and utilizes an end-to-end trainable neural network with a structure similar to Unet for dehazing. Dehamer [1] introduces a three-dimensional positional embedding module into the Transformer, incorporating priors related to haze density to estimate the haze density in different spatial regions. Trinity-Net [2] consists of three parameter estimation networks, each estimating haze thickness, ambient light, and medium transmission, respectively.

B. Data Augmentation

Data augmentation is an important technique [28] in deep learning, which mainly involves artificially increasing the amount of data by generating new data samples from existing data. Previous image data augmentation operations often increase the size of the dataset by altering the image shape or visual appearance. Common techniques include injecting noise, flipping, cropping, resizing, and color space operations [29]–[31]. Current data augmentation methods also include techniques based on image erasure. Cutout [32] is a data augmentation technique that involves randomly erasing subregions during training and filling them with 0 or 255 in the image. Random erasing [33] is an augmentation method that randomly erases subregions in the image, similar to cropping. However, it also randomly determines whether to mask and decides the aspect ratio and size of the masked region. The key idea of Hide-and-Seek [34] is to divide the image into randomly sized uniform squares and randomly delete a random number of squares. When important information is hidden, it forces the neural network to learn relevant features.

Recently, non-single-image mixed data augmentation methods have become increasingly common techniques in data augmentation. Mixup [35] combines two randomly selected images and their corresponding labels, where the mixing ratio is determined by a mixing coefficient α . This method can improve the accuracy of the model. CutMix [36] addresses the problem of information and local feature loss. CutMix randomly selects a region from each image when mixing images. Then it combines them to form a mixed image after swapping these regions. Puzzle Mix [37] introduces a puzzle-based mixed data augmentation technique. This method focuses on

flexibly utilizing key information and basic statistical data of images, aiming to break the neural network’s reliance on existing data augmentation. RandomMix [38] aims to enhance the generalization performance of the model. It randomly selects mixed augmentations from a set of augmentations and applies them to the image, allowing the model to encounter different samples. However, directly using mixed data augmentation methods is not suitable for image dehazing tasks. Using mixed data augmentation methods directly alters the visual content of the original image, potentially resulting in the loss of crucial information during the dehazing process.

In image dehazing tasks, data augmentation operations often need to be designed specifically for the characteristics of images under hazy conditions. To address this issue, we propose an external data augmentation and an internal data augmentation method. This method can enhance the model’s ability to handle hazy images and improve its robustness.

C. Self-supervised Learning

Self-supervised learning (SSL) has achieved significant success in the field of computer vision [39]–[45]. It trains models by generating labels automatically, without the need for manually annotated datasets. Many researchers have proposed different solutions for creating pseudo-labels. For example, flipping images, cropping or merging image patches, etc. The key idea of self-supervised learning is to utilize the inherent structure and relationships within the data itself to learn effective feature representations. Self-supervised learning can be trained on large amounts of unlabeled data, which is highly valuable in fields like remote sensing image dehazing and natural image dehazing. This is because acquiring large amounts of labeled data is often expensive and time-consuming.

III. METHODOLOGY

As shown in Fig. 2, our proposed method consists of two parts: external data augmentor and internal data augmentor. Firstly, we propose an external data augmentation method to reduce the contrast differences between different hazy datasets. External data augmentor makes the augmented dataset approximate the target dataset in the color space. The augmented samples obtained by our method can better match the distribution of the target domain. To this end, dehaze networks trained with consistent yet more quantity of samples have the potential to show superior results.

Building upon the augmentation of different domain datasets externally, we further explore additional locally effective information by augmenting the dataset internally. The model becomes more robust by coordinating external and internal augmentation. For internal data augmentation, we introduce a weak-to-strong coordinated data augmentation self-supervised learning method to improve the local details of images. The model can focus more on the details of the images by calculating the difference between weakly and strongly augmented images.

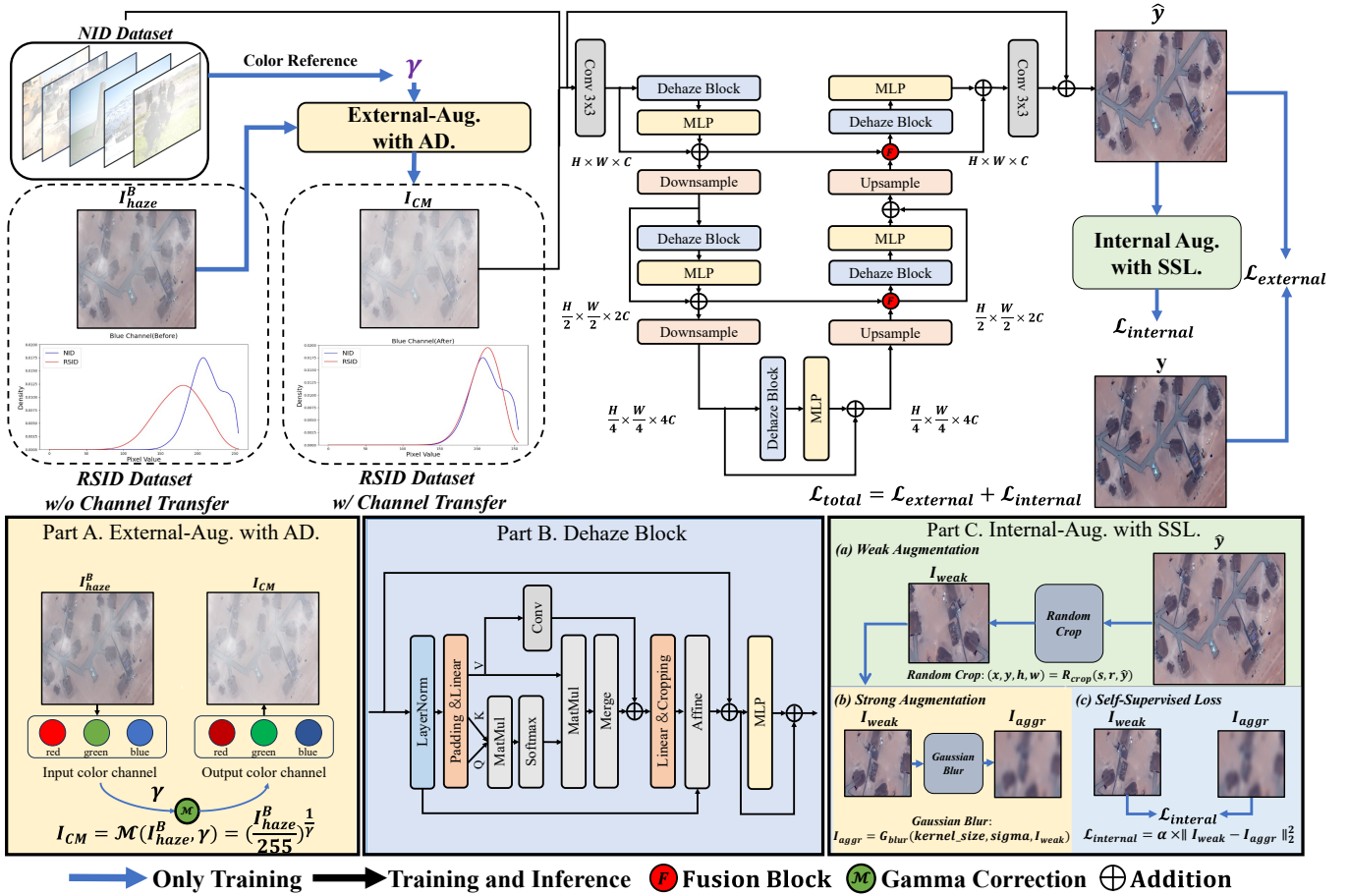


Fig. 2: Illustration of the proposed integrated framework for External-Augmentor with Auxiliary Datasets (External-Aug. with AD.) and Internal-Augmentor with Self-supervised Learning (Internal-Aug. with SSL.). Our method first performs augmentation on the external dataset to enrich dataset diversity. The external augmentor makes the auxiliary dataset be aligned with the target dataset in the color channels. Then, we apply the self-supervised learning method to augment the data internally. Specifically, the internal augmentor emphasizes attention to fine-grained details in images. By simultaneously augmenting the data externally and internally, our model achieves higher performance and robustness.

A. Cross-data External Augmentor for Alignment

As described in Sec. II, traditional data augmentation methods often rely on simple geometric and color transformations. However, this approach to processing images generated from the original dataset lacks diversity. Additionally, there are often significant differences between different dehaze datasets in terms of color and contrast. Suppose we directly use several datasets for joint training, the corresponding experiments often show a degradation.

In particular, we propose an external-augmentor to address the domain gap between different datasets. The proposed external-augmentor achieves efficient domain adaptation without an additional training phase. Specifically, we first calculate the gamma values $\gamma_{R,G,B}$ for the three channels to be transferred to the target domain. Then, we perform gamma calibration on the images to be transferred, as follows:

$$O_{R,G,B} = \mathcal{M}(I_{R,G,B}) = \left(\frac{I_{R,G,B}}{255} \right)^{\frac{1}{\gamma_{R,G,B}}} \quad (2)$$

where $I_{R,G,B}$ and $O_{R,G,B}$ represent the input and output pixel

intensities ($[0,255]$), respectively, and γ is the gamma factor. The subscripts R, G, B represent the color channels, and the values of different channels are unique. Our method adjusts the RSID dataset to make it more similar to the NID dataset from color space. As shown in Fig. 3, the RSID images better be aligned with the RGB distribution of the NID dataset after external augmentation. By using external augmentation, our method effectively expands the dataset's quantity and introduces external datasets, enriching the diversity of the dataset. Some of the transformed data is shown in Fig. 4. The first column shows the original RSID images, the second column shows the new RSID images after data preprocessing, and the third column shows the target dataset NID. As shown in Fig. 4, the RSID images become closer to the NID dataset after the external augmentor. To illustrate our method intuitively, we demonstrate the algorithmic flow of external augmentation. As shown in Algorithm 1, we apply the RSID dataset as an example to present the implementation of the channel correction.

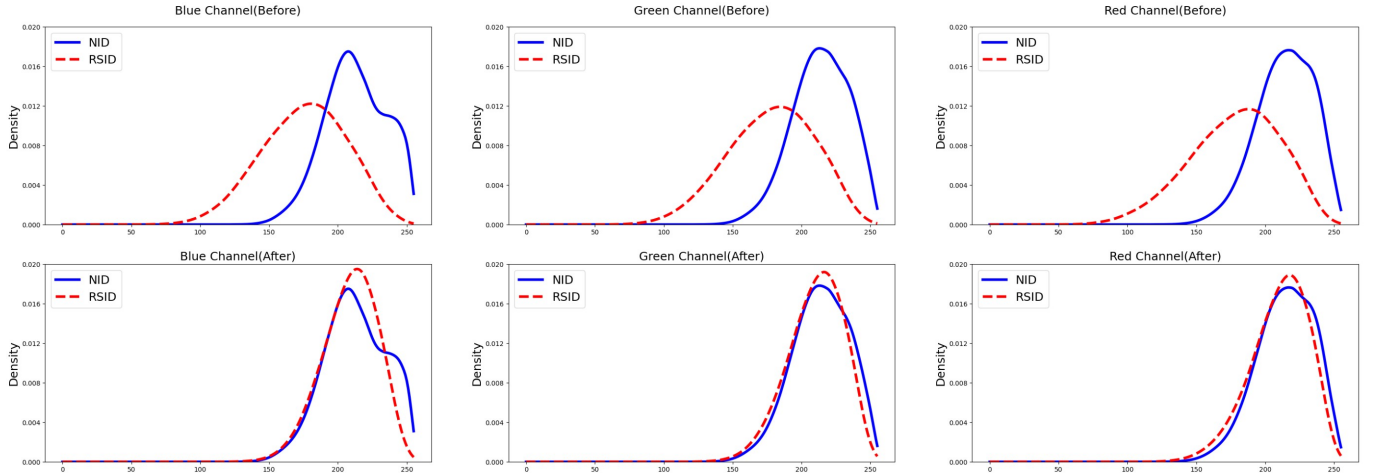


Fig. 3: A demonstration of domain gap between different dehazing datasets. We perform gamma correction on the RSID dataset based on the RGB values of the NID dataset. It can be observed that before correction, there is a significant difference between the distributions of the datasets in the RGB channels. After external data augmentation, the distributions of RSID images are closely aligned with those of NID images in the RGB channels.

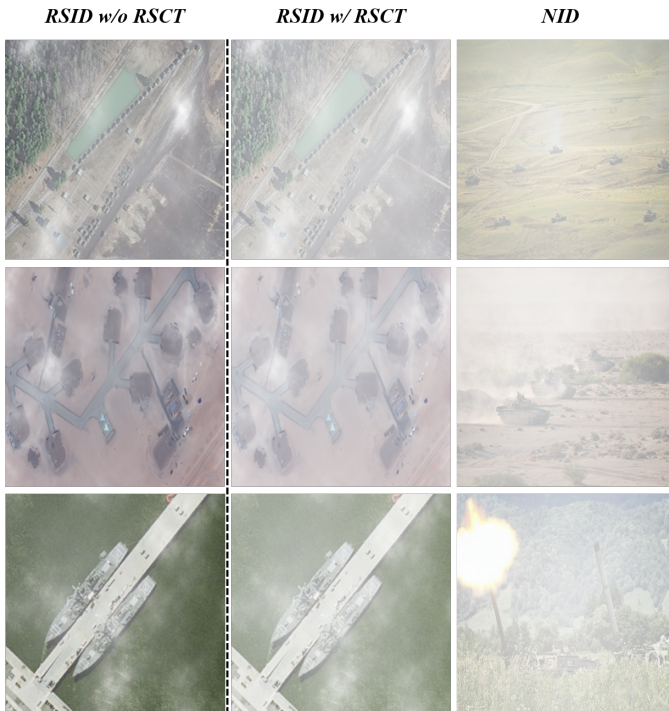


Fig. 4: Illustration of external augmentation. The RSID images become closer to the NID dataset by external augmentor.

B. Feature Extractor

As shown in Fig. 2, the dehazing network is composed of a 5-layer U-Net structure [46]. The network includes two downsampling and upsampling steps. In the network, the input hazy image passes through Dehaze Block modules and feature fusion modules to finally obtain the output dehazed image \hat{y} . As shown in part B of Fig. 2, in the Dehaze Block module, the input feature maps undergo normalization and padding layers. Then they are projected into Q, K, and

V (query, key, value) using linear layers, used to calculate attention scores [47]. Additionally, the Dehaze Block module applies multi-head self-attention within a window to handle relationships between image patches. It allows the dehazing network to consider correlations between different positions while extracting features. Thus, the model can learn structural information in the image more effectively to improve the model performance.

Different from directly integrating with the traditional U-Net network architecture, the feature fusion module learns channel attention weights of different feature maps through operations like global average pooling [48]. Thus, the network can dynamically adjust its contributions based on the importance of each feature map. In the feature fusion module, assuming there are two feature maps f_1 and f_2 , We project f_1 to f'_1 using a linear layer. We then use operations such as $GAP(\cdot)$ sequentially to obtain fusion weights w_1 and w_2 .

Next, we use the weights to fuse f'_1 and f_2 with the following additional short residual:

$$x = w_1 f'_1 + w_2 f_2 + f_2 \quad (3)$$

In the final short residual fusion stage, the two feature maps are fused through linear combination while introducing an additional short residual term. This design helps preserve the information from the original input while introducing the fused features. It allows the network to better utilize multi-scale and multi-level feature information, thus improving the accuracy and robustness of the dehazing effect.

Then, we use the \mathcal{L}_1 loss function to train the feature extractor, obtaining the loss for external data:

$$\mathcal{L}_{external} = |y - \hat{y}| \quad (4)$$

C. Internal-Augmentor with Self-supervised Learning

For the internal dataset, we propose an internal data augmentation strategy to improve the model's ability to preserve

Algorithm 1 External-Augmentor for Data Alignment

Input: $I_{haze} \in R^{N \times C \times H \times W}$:RSID origin hazy images
Intermediate parameter:
 $\gamma_R, \gamma_G, \gamma_B$: gamma transform values for channel migration
Output: $I_{CM} \in R^{N \times C \times H \times W}$:RSID hazy images after channel migration transformation

▷ Three channel color averages for the RSID origin hazy images
for $n \leftarrow 1$ to N **do**
 $Mean(I_{RSID-R}) = Mean(I_{RSID-R}^n)$
 $Mean(I_{RSID-G}) = Mean(I_{RSID-G}^n)$
 $Mean(I_{RSID-B}) = Mean(I_{RSID-B}^n)$
end for

▷ Three channel color averages for the NID hazy images
for $n \leftarrow 1$ to N **do**
 $Mean(I_{NID-R}) = Mean(I_{NID-R}^n)$
 $Mean(I_{NID-G}) = Mean(I_{NID-G}^n)$
 $Mean(I_{NID-B}) = Mean(I_{NID-B}^n)$
end for

▷ compute $\gamma_R, \gamma_G, \gamma_B$
 $Mean(I_{NID-R}) = \left(\frac{Mean(I_{RSID-R})}{255} \right)^{\frac{1}{\gamma_R}}$
 $Mean(I_{NID-G}) = \left(\frac{Mean(I_{RSID-G})}{255} \right)^{\frac{1}{\gamma_G}}$
 $Mean(I_{NID-B}) = \left(\frac{Mean(I_{RSID-B})}{255} \right)^{\frac{1}{\gamma_B}}$

▷ Get I_{CM}
for $n \leftarrow 1$ to N **do**
 $O_{CM-R} = \left(\frac{I_R}{255} \right)^{\frac{1}{\gamma_R}}$
 $O_{CM-G} = \left(\frac{I_G}{255} \right)^{\frac{1}{\gamma_G}}$
 $O_{CM-B} = \left(\frac{I_B}{255} \right)^{\frac{1}{\gamma_B}}$
end for
 Then we can get RSID hazy images after channel migration transformation

Algorithm 2 Internal-Augmentor with Self-supervised Learning

Input: \hat{y} : the results of the enhanced network, $\alpha=0.1$
Output: $\mathcal{L}_{internal}$: internal augmentation loss

for $i \leftarrow 1$ to I **do**
 $I_{weak} = P_{weak}(\hat{y})$
 $I_{aggr} = P_{aggr}(I_{weak})$
 $\mathcal{L}_{internal} = \alpha \times \|I_{weak} - I_{aggr}\|_2^2$
 $\alpha = \alpha \times \frac{1}{2} (\cos(\pi \frac{i}{I}) + 1)$
end for

details and contrast in dehazed images. Building upon external dataset augmentation, it emphasizes attention to local details in images, making the model more robust. Specifically, we applied different degrees of data augmentation to the output results \hat{y} of the augmentation model. This is represented as

follows:

$$I_{weak} = P_{weak}(\hat{y}) \quad (5)$$

Where $P_{weak}()$ represents a weak data augmentation operation, and I_{weak} denotes the image generated by performing weak augmentation on \hat{y} . Subsequently, we apply strong augmentation to I_{weak} , which is specifically represented as follows:

$$I_{aggr} = P_{aggr}(I_{weak}) \quad (6)$$

Where I_{aggr} is the image generated through strong augmentation based on I_{weak} , and P_{aggr} represents the strong augmentation operation. Specifically, weak augmentation refers to random cropping, and strong augmentation P_{aggr} is Gaussian blurring. Finally, we compute the L2 norm between I_{weak} and I_{aggr} , obtained through weak-strong augmentation to optimize the model's internal loss as:

$$\mathcal{L}_{internal} = \alpha \times \|I_{weak} - I_{aggr}\|_2^2 \quad (7)$$

$$\alpha = \alpha \times \frac{1}{2} \left(\cos\left(\pi \frac{s}{S}\right) + 1 \right), \quad (8)$$

where α is a hyperparameter that varies with cosine decay. In experiments, we set the initial value of $\alpha = 0.1$, s is the current training iteration and S is the total number of training iterations. By utilizing the self-supervised learning with $\mathcal{L}_{internal}$, we can obtain the internal similarity between data, which allows the model to learn richer features and be more robust.

As shown in Fig. 5, we visualize the difference in image quality with and without internal data augmentation. The first and last columns represent the hazy images and ground truth images, respectively. The second column shows the dehazed images obtained using the external data augmentation method. The third column shows dehazed images obtained using both external data augmentor and the strong-weak augmentation self-supervised learning (SW-SSL) approach for internal data augmentor. As shown in Fig. 5, by using the internal data augmentation self-supervised method, the details of the out-of-distribution image are closer to the real haze-free image.

In Algorithm 2, we present the implementation of strong-weak self-supervised augmentation on internal data.

D. Loss Function

The original dehazing loss compares the generated dehazed images with the ground truth haze-free images using L1 loss. Then, we incorporate the self-supervised loss obtained from the internal dataset into the original loss. Therefore, we obtain the total loss from both external and internal data as follows:

$$\mathcal{L}_{total} = \mathcal{L}_{external} + \mathcal{L}_{internal} \quad (9)$$

IV. EXPERIMENT

A. Experimental Settings

Our model is implemented using PyTorch 1.13.0 on an NVIDIA RTX 3090 GPU. The model is trained using the AdamW optimizer [49] with a cosine annealing strategy [50]. The batch size and training epochs are set to 8 and 3000, respectively. The learning rate is reduced from an initial rate of

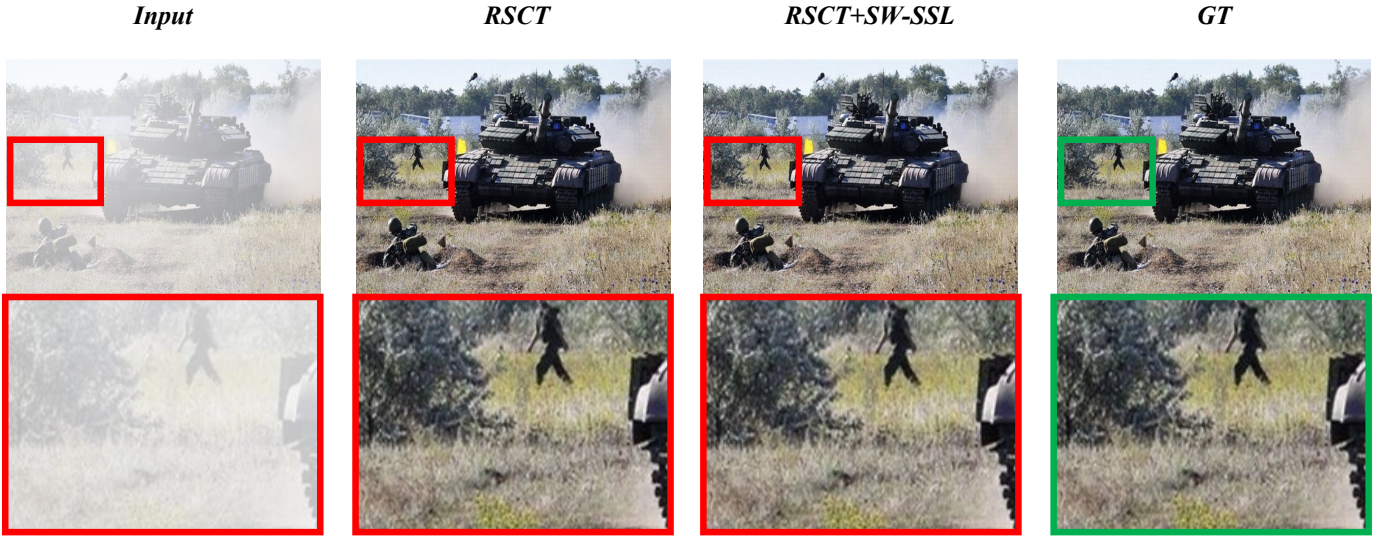


Fig. 5: Dehazed images obtained with and without internal data augmentor. The second column shows the dehazed images obtained only after applying RSID Channel Transformer (RSCT). The third column shows the dehazed images obtained after applying both RSID Channel Transformer and Strong-Weak Self-supervised Learning (RSCT+SW-SSL). It can be seen that the results obtained with internal augmentation have more prominent details, closely resembling the real haze-free image (GT).

1e-4 to 1e-6. Additionally, we apply the aforementioned external augmentation method to the RSID dataset. Subsequently, we incorporate the revised RSID dataset as an augmented dataset into the NID dataset for training.

B. Dataset

For dataset comparison, we select two datasets:

The NID [2] consists of synthetic natural hazy images. It relies on the estimation of depth information. Therefore, the NID dataset first uses a depth prediction algorithm to estimate the depth maps of natural images. Then, natural hazy images are synthesized based on a haze simulation strategy. The NID consists of 1000 pairs of hazy-real image pairs.

The RSID [2] consists of 1000 pairs of hazy-real remote sensing image pairs. The RSID is generated based on extensive statistical information on haze parameters. Parameters such as ambient light $A \in [0.7, 1]$, medium transmittance $t \in [0.25, 0.65]$, and haze thickness $s \in [0.35, 0.75]$ are randomly sampled to generate samples with varying visibility. Specifically, we use the RSID as an augmented dataset and apply the channel migration method to it. We respectively select 300 and 900 images from the RSID to transfer to the NID for data augmentation. Therefore, we finally obtained the augmented datasets RSID_Transfer3:1 (RSCT 3:1) and RSID_Transfer1:1 (RSCT 1:1).

For the NID, we select the first 900 images in the order of arrangement as the training set, while the remaining 100 images are used as the test set (N100). Therefore, for the RSCT 3:1 dataset, a total of 1200 images are used as the training set. For the RSCT 1:1 dataset, a total of 1800 images are used as the training set.

C. Evaluation Metrics and Comparison Objects

To evaluate our method's performance, we adopt Peak Signal-to-Noise Ratio (PSNR) and Structural Similarity Index (SSIM) as evaluation metrics. These metrics are commonly used as standards for evaluating image quality in image dehazing tasks.

PSNR (Peak Signal to Noise Ratio) is an objective measure for evaluating image quality. A higher value indicates better image quality, and it's commonly used to quantify the visual difference between two images. Here, it represents the difference between the resulting dehazed image and the ground truth haze-free image.

$$PSNR = 10 \times \log_{10} \left(\frac{MAX^2}{MSE} \right), \quad (10)$$

where MAX is the possible maximum pixel value in the image. MSE stands for Mean Squared Error, which represents the average of the squared differences between the pixel values of the true clear image and the dehazed image.

SSIM (Structural Similarity Index) is another metric used to measure the quality of images. The SSIM metric considers three aspects of similarity in images: luminance, contrast, and structure. Its calculation formula is as follows:

$$SSIM(a, b) = \frac{(2\mu_a\mu_b + c_1)(2\sigma_{ab} + c_2)}{(\mu_a^2 + \mu_b^2 + c_1)(\sigma_a^2 + \sigma_b^2 + c_2)}, \quad (11)$$

where a and b represent two images. μ_a and μ_b are the mean values of the images. σ_a^2 and σ_b^2 are the variances of the images. σ_{ab} is the covariance between the two images. The SSIM value ranges between -1 and 1, where a value closer to 1 indicates greater similarity between the two images.

D. Comparison with Baseline Methods

We compare our method with state-of-the-art dehazing works. The experiments show that our results are significantly

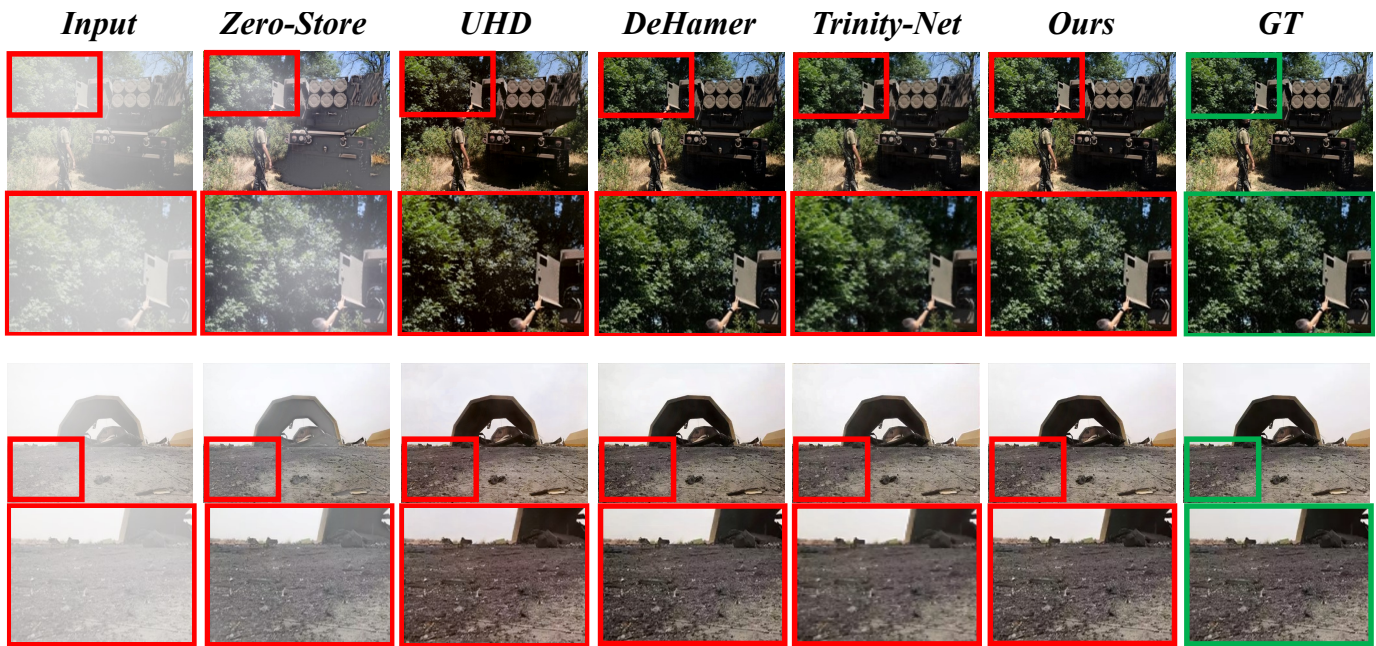


Fig. 6: Dehazed Images Obtained by Different Methods on the NID

TABLE I: Quantitative Results on the NID

Method	$PSNR \uparrow$	$SSIM \uparrow$
DEFADE [11]	15.80	0.8383
GDCP [6]	15.99	0.7433
zero-store [51]	16.09	0.7849
ROP [9]	16.39	0.8087
TCN [52]	16.36	0.7112
Haze-Lines [53]	17.96	0.8378
ALC [8]	19.03	0.8499
ZID [54]	19.62	0.8270
DeHamer [1]	23.11	0.9369
UHD [12]	23.72	0.9182
Trinity-Net [2]	28.80	0.9743
Ours	31.14	0.9896

TABLE II: Quantitative Results on the RSID

Method	$PSNR \uparrow$	$SSIM \uparrow$
IDeRs [55]	13.60	0.6439
TCN [52]	14.21	0.6058
GRS-HTM [56]	14.80	0.5190
ROP [9]	15.57	0.7500
EVPM [57]	15.58	0.6889
SDCP [58]	16.05	0.6913
STD [59]	16.26	0.5592
zero-store [51]	16.65	0.7173
ZID [54]	18.99	0.7267
UHD [12]	22.06	0.8891
DeHamer [1]	23.61	0.8990
Trinity-Net [2]	23.78	0.9224
Ours	25.44	0.9399

better than other methods, as shown in Tab. I with specific experimental results.

Observing Tab. I, we can see that our method first achieves a PSNR metric reaching 31.14. Moreover, it significantly outperforms other methods in terms of both PSNR and SSIM metrics. We observe that our method achieves a PSNR improvement of 2.34 dB compared to the Trinity-Net [2]. After our method, its SSIM value has increased by 0.0153 compared to Trinity-Net's 0.9743. Compared to the UHD [12], our method has improved by 7.42 dB in terms of PSNR and 0.0714 in terms of SSIM. These results indicate that our method is better at restoring image visibility.

As shown in Fig. 6, to specifically demonstrate the superior-

ity of our method, we compared our model results with other methods. The first column represents the hazy image. The second, third, fourth, and fifth columns respectively depict the dehazed images obtained by the Zero-store [51], UHD [12], DeHamer [1], and Trinity-Net [2] methods. The sixth column displays the dehazed image achieved through our method. The last column shows the ground truth haze-free image. We compare the dehazed images obtained by our method with those obtained by other methods on the N100 test set. For example, from the images obtained above, it can be seen that our method approaches the real image more closely in terms of texture details. From the zoomed-in images, it can be observed

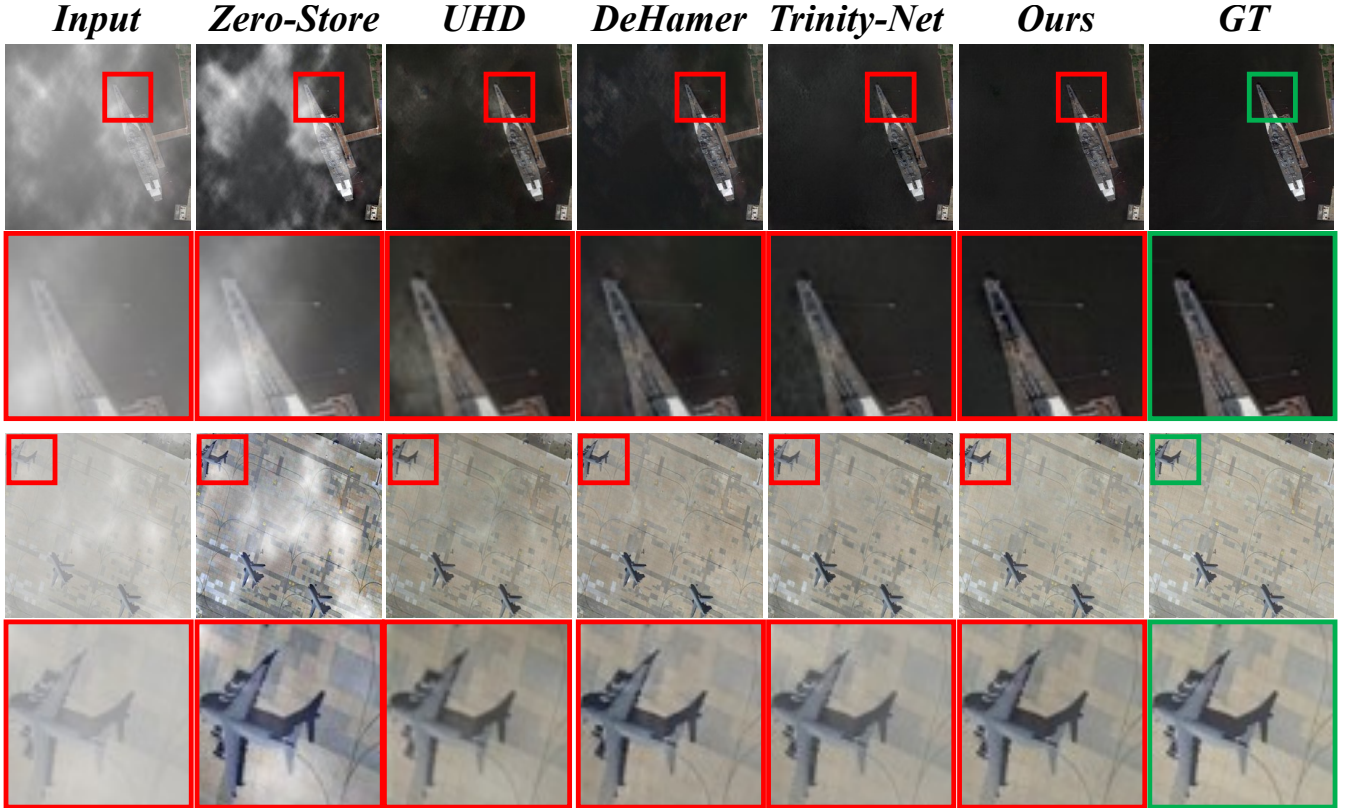


Fig. 7: Dehazed Images Obtained by Different Methods on the RSID

TABLE III: Ablation Study Using Only Internal Data Augmentation and Self-Supervised Module

Internal-augmentor SW-SSL	N100	
	$PSNR \uparrow$	$SSIM \uparrow$
×	30.06	0.9871
✓	30.20	0.9875

TABLE IV: Ablation Study Using Only External Data Augmentation

External-augmentor		N100	
RSCT3:1	RSCT1:1	$PSNR \uparrow$	$SSIM \uparrow$
×	×	30.06	0.9871
✓	×	30.47	0.9878
×	✓	30.71	0.9892

that our dehazed images are noticeably closer to the real haze-free images in terms of texture and color. Moreover, the edge details are clearer compared to the Trinity-Net [2] method.

We also apply our method to the remote sensing dataset RSID. Fig. 7, Fig. 8 specifically illustrates the comparison between our method and other methods. From the figures, it can be seen that the dehazed images obtained by the zero-store method [51] still contain haze, while the dehazed images obtained by the UHD method [12] exhibit partial distortion in

TABLE V: Ablation study using both external and internal data augmentation methods

External-augmentor and Internal-augmentor			N100	
SW-SSL	RSCT3:1	RSCT1:1	$PSNR \uparrow$	$SSIM \uparrow$
×	×	×	30.06	0.9871
✓	✓	×	30.70	0.9896
✓	×	✓	31.14	0.9896

terms of color. In comparison to DeHamer [1], in the results shown in the fourth column, there is still a small amount of residual haze along the edges. In comparison to Trinity-Net [2], in the results shown in the fifth column, Trinity-Net [2] results exhibit differences in local color compared to the ground truth haze-free image. In our method, the haze has been removed, and there is no distortion in color. The dehazed images obtained through our method are closest to the real haze-free images.

In Tab. II, we observe that our method outperforms other methods significantly in both PSNR and SSIM metrics. For the zero-store [51], UHD [12], DeHamer [1], and Trinity-Net methods [2], we obtained actual quantitative results through reproduction. The experimental results of other methods are obtained based on the Trinity-Net [2] paper. Compared to Trinity-Net [2], our method achieved an improvement of 1.66 dB in the quantitative metric PSNR and an improvement of 0.0175 in SSIM. Compared to DeHamer [1], our method achieved an improvement of 1.83 dB in the quantitative

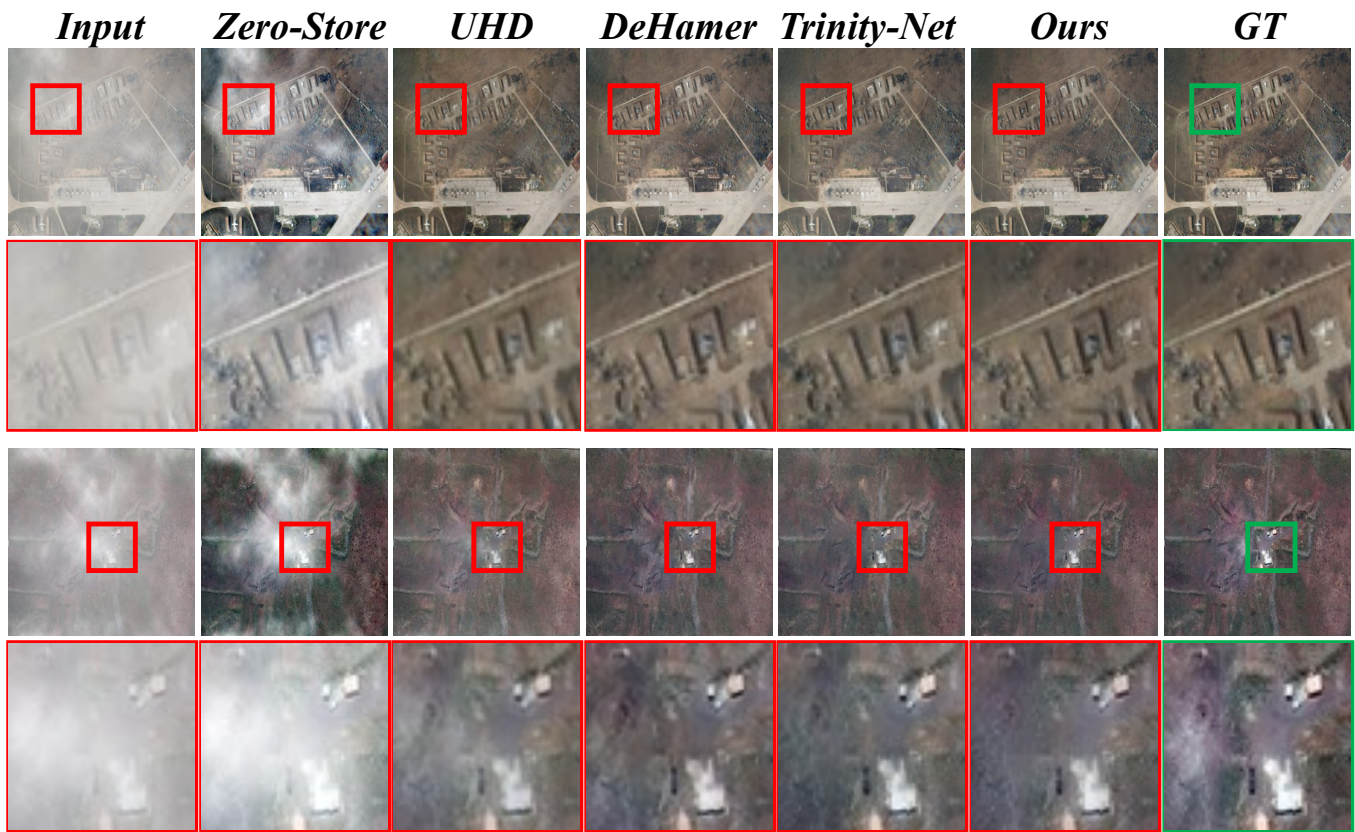


Fig. 8: Dehazed Images Obtained by Different Methods on the RSID

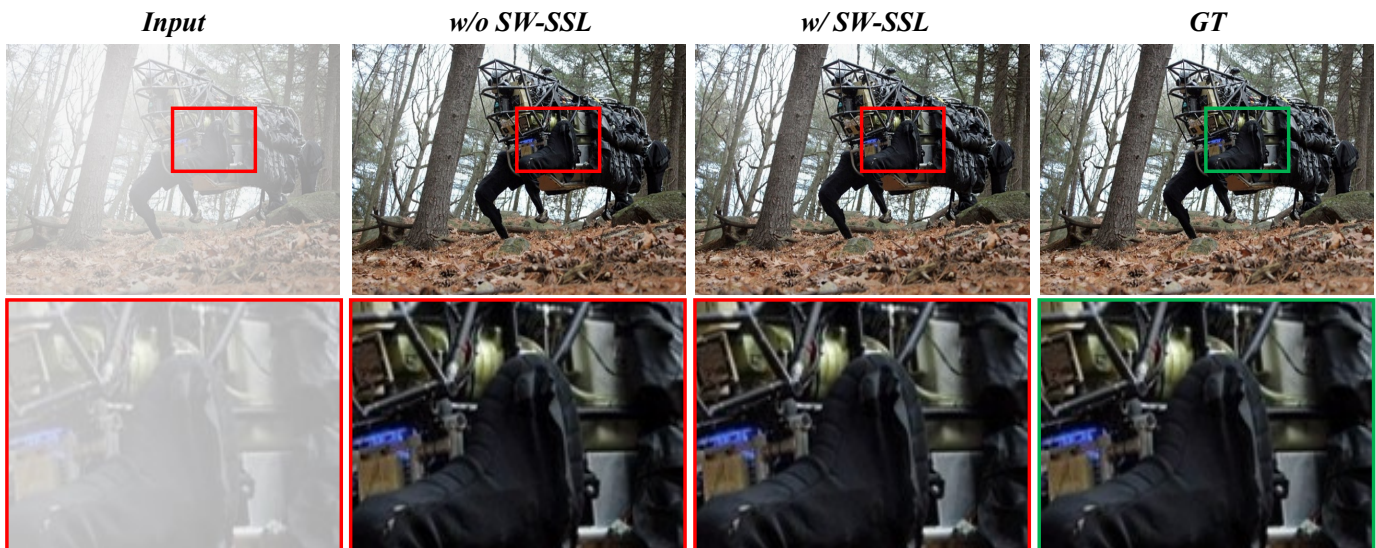


Fig. 9: Dehazed Images Obtained After Internal Data Augmentation and Self-Supervised Module. The second column shows the dehazed images obtained without applying Strong-Weak Self-supervised Learning (w/o SW-SSL). The third column shows the dehazed images obtained after applying Strong-Weak Self-supervised Learning (w/ SW-SSL).

metric PSNR and an improvement of 0.0409 in SSIM. These quantitative results indicate that our method also produces dehazed images with higher visual quality on the remote sensing dataset RSID.

E. Ablation Study

To demonstrate the effectiveness of our proposed method, we conduct ablation studies to analyze the effects of different modules, including external data augmentation, internal data augmentation, and self-supervised methods. We add different



Fig. 10: Dehazed images obtained using external data augmentation method with ratios of 3:1 and 1:1 respectively. The second column shows the dehazed images obtained without applying RSCT (w/o RSCT). The third column shows the dehazed images obtained after applying RSCT with ratios of 3:1 (w/RSCT 3:1). The fourth column shows the dehazed images obtained after applying RSCT with ratios of 1:1 (w/RSCT 1:1).



Fig. 11: Dehazed images obtained using both external and internal data augmentation methods. The second column shows the dehazed images obtained without applying RSCT and SW-SSL (w/o RSCT+SW-SSL). The third column shows the dehazed images obtained after applying RSCT with ratios of 3:1 and SW-SSL (w/RSCT3:1+SW-SSL). The fourth column shows the dehazed images obtained after applying RSCT with ratios of 1:1 and SW-SSL (w/RSCT1:1+SW-SSL).

modules to the network, including: (1) Only using internal data augmentation and self-supervised method. (2) Only using external data augmentation method. (3) Using both external data augmentation method and internal data augmentation and self-supervised method simultaneously.

We use L1 loss as the initial image reconstruction loss (Eq. 4), while in the self-supervised method, we use $\mathcal{L}_{internal}$ loss. We use the remaining one hundred images from the NID dataset (NID100) as the test set. The summary of the metrics for these models is presented in the following table.

In Tab. III, we only used internal data augmentation and a self-supervised module in our method. Compared to not adding modules, using internal data augmentation and self-supervised modules results in an improvement of 0.14 dB in PSNR values on NID100. In Fig. 9, partial dehazed images obtained after internal data augmentation and self-supervised modules are shown.

In Tab. IV, we solely employ external data augmentation in

the model. Specifically, we incorporate external data augmentation by including the augmented RSID dataset in the training set. The training images from the NID dataset and the RSID dataset are divided into a ratio of 3:1 and 1:1, respectively, for training. In Tab. IV, compared to the results obtained without adding any modules, the results obtained with a 1:1 ratio show improvements of 0.65dB and 0.0021 in PSNR and SSIM metrics, respectively. Compared to the 3:1 ratio, the 1:1 ratio shows improvements of 0.24 and 0.0014 in PSNR and SSIM metrics, respectively. To some extent, it indicates that appropriately augmenting the dataset can make the model more robust. Fig. 10 shows the experimental results of haze removal with external data augmentation at ratios of 3:1 and 1:1, respectively.

Then, we train the network using both external and internal augmentation methods simultaneously, as shown in Tab. V. We observe that the highest PSNR value of 31.14dB is achieved when simultaneously using the weak-strong augmentation self-

supervised method and dividing the training data of NID and RSID in a 1:1 ratio during the channel transfer module. Compared to the results obtained without adding any modules, the PSNR value on the test set has increased by 1.08dB, and the SSIM has increased by 0.0025. Compared to the 3:1 split of training data between NID and RSID, the PSNR on the test set obtained through the 1:1 split has increased by 0.44dB. As shown in Fig. 11, the single dehazed image obtained after applying both modules exhibits higher visual quality and is closer to the true haze-free image in terms of overall color.

V. CONCLUSION

In this paper, we propose a novel method that performs data augmentation separately on the external and internal aspects of the data. Specifically, we achieve external data augmentation using channel transfer and internal data augmentation using strong-weak augmentation self-supervised learning. Our method leverages data diversity at the external level and further explores internal information to effectively dehaze images. Experimental results show that our method achieves outstanding performance after applying both internal and external data augmentation methods. Compared to other advanced methods, our method performs better in terms of PSNR and SSIM metrics on both the Natural Image Dataset (NID) and the Remote Sensing Image Dataset (RSID). The resulting dehazed images also contain rich details and closely resemble the ground truth haze-free images.

REFERENCES

- [1] C.-L. Guo, Q. Yan, S. Anwar, R. Cong, W. Ren, and C. Li, "Image dehazing transformer with transmission-aware 3d position embedding," in *Proceedings of the IEEE/CVF conference on computer vision and pattern recognition*, 2022, pp. 5812–5820.
- [2] K. Chi, Y. Yuan, and Q. Wang, "Trinity-net: Gradient-guided swin transformer-based remote sensing image dehazing and beyond," *IEEE Transactions on Geoscience and Remote Sensing*, vol. 61, pp. 1–14, 2023.
- [3] E. J. McCartney, "Optics of the atmosphere: scattering by molecules and particles," *New York*, 1976.
- [4] S. K. Nayar and S. G. Narasimhan, "Vision in bad weather," in *Proceedings of the seventh IEEE international conference on computer vision*, vol. 2. IEEE, 1999, pp. 820–827.
- [5] S. G. Narasimhan and S. K. Nayar, "Vision and the atmosphere," *International journal of computer vision*, vol. 48, pp. 233–254, 2002.
- [6] Y.-T. Peng, K. Cao, and P. C. Cosman, "Generalization of the dark channel prior for single image restoration," *IEEE Transactions on Image Processing*, vol. 27, no. 6, pp. 2856–2868, 2018.
- [7] K. He, J. Sun, and X. Tang, "Single image haze removal using dark channel prior," *IEEE transactions on pattern analysis and machine intelligence*, vol. 33, no. 12, pp. 2341–2353, 2010.
- [8] Y.-T. Peng, Z. Lu, F.-C. Cheng, Y. Zheng, and S.-C. Huang, "Image haze removal using airlight white correction, local light filter, and aerial perspective prior," *IEEE Transactions on Circuits and Systems for Video Technology*, vol. 30, no. 5, pp. 1385–1395, 2019.
- [9] J. Liu, R. W. Liu, J. Sun, and T. Zeng, "Rank-one prior: Real-time scene recovery," *IEEE Transactions on Pattern Analysis and Machine Intelligence*, 2022.
- [10] Y. Wang, X. Yan, D. Guan, M. Wei, Y. Chen, X.-P. Zhang, and J. Li, "Cycle-snsrgan: Towards real-world image dehazing via cycle spectral normalized soft likelihood estimation patch gan," *IEEE Transactions on Intelligent Transportation Systems*, vol. 23, no. 11, pp. 20368–20382, 2022.
- [11] L. K. Choi, J. You, and A. C. Bovik, "Referenceless prediction of perceptual fog density and perceptual image defogging," *IEEE Transactions on Image Processing*, vol. 24, no. 11, pp. 3888–3901, 2015.
- [12] Z. Zheng, W. Ren, X. Cao, X. Hu, T. Wang, F. Song, and X. Jia, "Ultra-high-definition image dehazing via multi-guided bilateral learning," in *2021 IEEE/CVF Conference on Computer Vision and Pattern Recognition (CVPR)*. IEEE, 2021, pp. 16180–16189.
- [13] M. Wang, Y. Song, P. Wei, X. Xian, Y. Shi, and L. Lin, "Idf-cr: Iterative diffusion process for divide-and-conquer cloud removal in remote-sensing images," *IEEE Transactions on Geoscience and Remote Sensing*, 2024.
- [14] X. Xian, Q. Zhou, J. Qin, X. Yang, Y. Tian, Y. Shi, and D. Tian, "Croze: Low-light enhancement by cross-sensor interaction for nighttime driving scenes," *Expert Systems with Applications*, vol. 248, p. 123470, 2024.
- [15] Y. Shi, H. Li, S. Zhang, Z. Yang, and X. Wang, "Criteria comparative learning for real-scene image super-resolution," *IEEE Transactions on Circuits and Systems for Video Technology*, vol. 32, no. 12, pp. 8476–8485, 2022.
- [16] H. Li, J. Qin, Z. Yang, P. Wei, J. Pan, L. Lin, and Y. Shi, "Real-world image super-resolution by exclusionary dual-learning," *IEEE Transactions on Multimedia*, vol. 25, pp. 4752–4763, 2022.
- [17] C. Zhang, K.-M. Lam, and Q. Wang, "Cof-net: A progressive coarse-to-fine framework for object detection in remote-sensing imagery," *IEEE Transactions on Geoscience and Remote Sensing*, vol. 61, pp. 1–17, 2023.
- [18] X. Yang, Y. Wang, N. Wang, and X. Gao, "An enhanced siammask network for coastal ship tracking," *IEEE Transactions on Geoscience and Remote Sensing*, vol. 60, pp. 1–11, 2021.
- [19] Z. Li, Y. Sun, L. Zhang, and J. Tang, "Ctnet: Context-based tandem network for semantic segmentation," *IEEE Transactions on Pattern Analysis and Machine Intelligence*, vol. 44, no. 12, pp. 9904–9917, 2021.
- [20] Z. Peng, Z. Li, J. Zhang, Y. Li, G.-J. Qi, and J. Tang, "Few-shot image recognition with knowledge transfer," in *Proceedings of the IEEE/CVF international conference on computer vision*, 2019, pp. 441–449.
- [21] Q. Zhu, J. Mai, and L. Shao, "A fast single image haze removal algorithm using color attenuation prior," *IEEE transactions on image processing*, vol. 24, no. 11, pp. 3522–3533, 2015.
- [22] R. Fattal, "Dehazing using color-lines," *ACM transactions on graphics (TOG)*, vol. 34, no. 1, pp. 1–14, 2014.
- [23] D. Berman, S. Avidan *et al.*, "Non-local image dehazing," in *Proceedings of the IEEE conference on computer vision and pattern recognition*, 2016, pp. 1674–1682.
- [24] B. Cai, X. Xu, K. Jia, C. Qing, and D. Tao, "Dehazenet: An end-to-end system for single image haze removal," *IEEE transactions on image processing*, vol. 25, no. 11, pp. 5187–5198, 2016.
- [25] W. Ren, S. Liu, H. Zhang, J. Pan, X. Cao, and M.-H. Yang, "Single image dehazing via multi-scale convolutional neural networks," in *Computer Vision—ECCV 2016: 14th European Conference, Amsterdam, The Netherlands, October 11–14, 2016, Proceedings, Part II 14*. Springer, 2016, pp. 154–169.
- [26] H. Zhang and V. M. Patel, "Densely connected pyramid dehazing network," in *Proceedings of the IEEE conference on computer vision and pattern recognition*, 2018, pp. 3194–3203.
- [27] W. Ren, L. Ma, J. Zhang, J. Pan, X. Cao, W. Liu, and M.-H. Yang, "Gated fusion network for single image dehazing," in *Proceedings of the IEEE conference on computer vision and pattern recognition*, 2018, pp. 3253–3261.
- [28] Y. Liu, H. Liu, L. Li, Z. Wu, and J. Chen, "A data-centric solution to nonhomogeneous dehazing via vision transformer," in *Proceedings of the IEEE/CVF Conference on Computer Vision and Pattern Recognition*, 2023, pp. 1406–1415.
- [29] S. Gidaris, P. Singh, and N. Komodakis, "Unsupervised representation learning by predicting image rotations," *arXiv preprint arXiv:1803.07728*, 2018.
- [30] M. Noroozi and P. Favaro, "Unsupervised learning of visual representations by solving jigsaw puzzles," in *European conference on computer vision*. Springer, 2016, pp. 69–84.
- [31] R. Zhang, P. Isola, and A. A. Efros, "Colorful image colorization," in *Computer Vision—ECCV 2016: 14th European Conference, Amsterdam, The Netherlands, October 11–14, 2016, Proceedings, Part III 14*. Springer, 2016, pp. 649–666.
- [32] T. DeVries and G. W. Taylor, "Improved regularization of convolutional neural networks with cutout," *arXiv preprint arXiv:1708.04552*, 2017.
- [33] Z. Zhong, L. Zheng, G. Kang, S. Li, and Y. Yang, "Random erasing data augmentation," in *Proceedings of the AAAI conference on artificial intelligence*, vol. 34, no. 07, 2020, pp. 13001–13008.
- [34] K. K. Singh, H. Yu, A. Sarmasi, G. Pradeep, and Y. J. Lee, "Hide-and-seek: A data augmentation technique for weakly-supervised localization and beyond," *arXiv preprint arXiv:1811.02545*, 2018.

- [35] H. Zhang, M. Cisse, Y. N. Dauphin, and D. Lopez-Paz, “mixup: Beyond empirical risk minimization,” *arXiv preprint arXiv:1710.09412*, 2017.
- [36] S. Yun, D. Han, S. J. Oh, S. Chun, J. Choe, and Y. Yoo, “Cutmix: Regularization strategy to train strong classifiers with localizable features,” in *Proceedings of the IEEE/CVF international conference on computer vision*, 2019, pp. 6023–6032.
- [37] J.-H. Kim, W. Choo, and H. O. Song, “Puzzle mix: Exploiting saliency and local statistics for optimal mixup,” in *International Conference on Machine Learning*. PMLR, 2020, pp. 5275–5285.
- [38] X. Liu, F. Shen, J. Zhao, and C. Nie, “Randomix: a mixed sample data augmentation method with multiple mixed modes,” *Multimedia Tools and Applications*, pp. 1–17, 2024.
- [39] J.-J. Hwang, S. X. Yu, J. Shi, M. D. Collins, T.-J. Yang, X. Zhang, and L.-C. Chen, “Segsort: Segmentation by discriminative sorting of segments,” in *Proceedings of the IEEE/CVF International Conference on Computer Vision*, 2019, pp. 7334–7344.
- [40] X. Zhang and M. Maire, “Self-supervised visual representation learning from hierarchical grouping,” *Advances in Neural Information Processing Systems*, vol. 33, pp. 16 579–16 590, 2020.
- [41] P. O. O Pinheiro, A. Almahairi, R. Benmalek, F. Golemo, and A. C. Courville, “Unsupervised learning of dense visual representations,” *Advances in Neural Information Processing Systems*, vol. 33, pp. 4489–4500, 2020.
- [42] Z. Wang, Q. Li, G. Zhang, P. Wan, W. Zheng, N. Wang, M. Gong, and T. Liu, “Exploring set similarity for dense self-supervised representation learning,” in *Proceedings of the IEEE/CVF Conference on Computer Vision and Pattern Recognition*, 2022, pp. 16 590–16 599.
- [43] M. Caron, I. Misra, J. Mairal, P. Goyal, P. Bojanowski, and A. Joulin, “Unsupervised learning of visual features by contrasting cluster assignments,” *Advances in neural information processing systems*, vol. 33, pp. 9912–9924, 2020.
- [44] A. Ermolov, A. Siarohin, E. Sangineto, and N. Sebe, “Whitening for self-supervised representation learning,” in *International conference on machine learning*. PMLR, 2021, pp. 3015–3024.
- [45] M. Zheng, S. You, F. Wang, C. Qian, C. Zhang, X. Wang, and C. Xu, “Ressl: Relational self-supervised learning with weak augmentation,” *Advances in Neural Information Processing Systems*, vol. 34, pp. 2543–2555, 2021.
- [46] Y. Song, Z. He, H. Qian, and X. Du, “Vision transformers for single image dehazing,” *IEEE Transactions on Image Processing*, vol. 32, pp. 1927–1941, 2023.
- [47] Z. Liu, Y. Lin, Y. Cao, H. Hu, Y. Wei, Z. Zhang, S. Lin, and B. Guo, “Swin transformer: Hierarchical vision transformer using shifted windows,” in *Proceedings of the IEEE/CVF international conference on computer vision*, 2021, pp. 10 012–10 022.
- [48] X. Li, W. Wang, X. Hu, and J. Yang, “Selective kernel networks,” in *Proceedings of the IEEE/CVF conference on computer vision and pattern recognition*, 2019, pp. 510–519.
- [49] I. Loshchilov and F. Hutter, “Decoupled weight decay regularization,” *arXiv preprint arXiv:1711.05101*, 2017.
- [50] Loshchilov, Ilya and Hutter, Frank, “Sgdr: Stochastic gradient descent with warm restarts,” *arXiv preprint arXiv:1608.03983*, 2016.
- [51] A. Kar, S. K. Dhara, D. Sen, and P. K. Biswas, “Zero-shot single image restoration through controlled perturbation of koschmieder’s model,” in *Proceedings of the IEEE/CVF Conference on Computer Vision and Pattern Recognition*, 2021, pp. 16 205–16 215.
- [52] J. Shin, H. Park, and J. Paik, “Region-based dehazing via dual-supervised triple-convolutional network,” *IEEE Transactions on Multimedia*, vol. 24, pp. 245–260, 2021.
- [53] D. Berman, T. Treibitz, and S. Avidan, “Single image dehazing using haze-lines,” *IEEE transactions on pattern analysis and machine intelligence*, vol. 42, no. 3, pp. 720–734, 2018.
- [54] B. Li, Y. Gou, J. Z. Liu, H. Zhu, J. T. Zhou, and X. Peng, “Zero-shot image dehazing,” *IEEE Transactions on Image Processing*, vol. 29, pp. 8457–8466, 2020.
- [55] L. Xu, D. Zhao, Y. Yan, S. Kwong, J. Chen, and L.-Y. Duan, “Iders: Iterative dehazing method for single remote sensing image,” *Information Sciences*, vol. 489, pp. 50–62, 2019.
- [56] Q. Liu, X. Gao, L. He, and W. Lu, “Haze removal for a single visible remote sensing image,” *Signal Processing*, vol. 137, pp. 33–43, 2017.
- [57] J. Han, S. Zhang, N. Fan, and Z. Ye, “Local patchwise minimal and maximal values prior for single optical remote sensing image dehazing,” *Information Sciences*, vol. 606, pp. 173–193, 2022.
- [58] J. Li, Q. Hu, and M. Ai, “Haze and thin cloud removal via sphere model improved dark channel prior,” *IEEE Geoscience and Remote Sensing Letters*, vol. 16, no. 3, pp. 472–476, 2018.
- [59] Z. Mi, Y. Li, J. Jin, Z. Liang, and X. Fu, “A generalized enhancement framework for hazy images with complex illumination,” *IEEE Geoscience and Remote Sensing Letters*, vol. 19, pp. 1–5, 2021.